A Transfer Matrix approach
to the Enumeration of Colored Links

J. L. Jacobsen *and* P. Zinn-Justin

Laboratoire de Physique Théorique et Modèles Statistiques
Université Paris-Sud, Bâtiment 100
91405 Orsay Cedex, France

We propose a transfer matrix algorithm for the enumeration of alternating link and tangle diagrams, giving a weight n to each connected component. Considering more general tetravalent diagrams with self-intersections and tangencies allows us to treat topological (flype) equivalences. This is done by means of a finite renormalization scheme for an associated matrix model. We give results, expressed as polynomials in n, for the various generating functions up to order 19 (2-legged tangle diagrams), 15 (4-legged tangles) and 11 (6-legged tangles) crossings. The limit $n \to \infty$ is solved explicitly. We then analyze the large-order asymptotics of the generating functions. For $0 \leq n \leq 2$ good agreement is found with a conjecture for the critical exponent, based on the KPZ relation.

1. Introduction

It is well-known that a d-dimensional system in statistical mechanics can be conceived as a $(d-1)$-dimensional quantum field theory, by distinguishing one of the spatial coordinates as the direction of time. This correspondence lies at the heart of the *transfer matrix* formalism, where a linear operator is used to describe the discrete time evolution of the corresponding quantum system. More generally, transfer matrices have numerous applications for the combinatorial enumeration of discrete objects for which a definite direction (the transfer, or time, direction) can be singled out. Recently, this combinatorial aspect has come into focus through the enumeration of various objects pertaining to two-dimensional quantum gravity [1,2,3,4], such as plane meanders. Common to these examples is the existence of a preferred direction (e.g. the river, in the case of meanders), which can be straightforwardly promoted to the time direction.

In a previous paper [4] we have shown how this scheme also applies to the enumeration of alternating knot diagrams. Here the knot itself defines the transfer direction, since the algorithm essentially consists in reading the knot starting from one "ingoing" leg and ending at the other "outgoing" leg.

It is however far from obvious how this principle may generalize to the case of *link diagrams* with more than one connected component. This is the purpose of the present paper. More specifically, the final goal is to count alternating tangles *at fixed number of connected components*; it is therefore a generalization of the counting of alternating tangles with minimum number of components done in [4], but also of the counting of alternating tangles of [5,6] and of oriented alternating tangles of [7]. We also present some results for tangles with a higher number of outgoing strings ("external legs"), instead of just four as in the publications mentioned above. We shall in what follows present not just one, but two rather different transfer matrices addressing this enumeration problem.

After the definitions in section 2, which include various intermediate generating functions needed in the calculation, we shall present in section 3 the basic ideas behind the two proposed transfer matrices for alternating tangle diagrams. Section 4 is devoted to more technical details on the actual implementation of these ideas on a computer, and section 5 gives the numerical results and their analysis. Finally, in Section 6, we discuss how our algorithms may be adapted to various other problems of interest in graph theory and statistical physics.
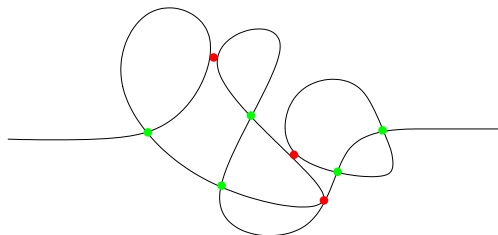
2. Definitions of the generating functions

The objects we want to consider are tangles with $2k$ "external legs", that is roughly speaking the data of k intervals embedded in a ball B and whose endpoints are given distinct points on the boundary ∂B, plus an arbitrary number of (unoriented) circles embedded in B, all intertwined, and considered up to orientation preserving homeomorphisms of B that reduce to the identity on ∂B. Tangles with 4 external legs will be simply called tangles. The rest of the basic definitions is identical to those given in [4]. We represent these objects using diagrams, and restrict ourselves to alternating diagrams. This implies in particular that tangles can be considered as flype equivalence classes of diagrams [8].

Our goal is to count the number of prime tangles with a certain number of external legs and connected components. We shall relate in this section their generating functions to a simpler, more directly computable quantity, which is the following triple generating function

$$G(n, g_1, g_2) = \sum_{k,p_1,p_2=0}^{\infty} a_{k,p_1,p_2} n^k g_1^{p_1} g_2^{p_2} \tag{2.1}$$

where a_{k,p_1,p_2} is the number of topologically inequivalent open curves in the plane going from $(-\infty, 0)$ to $(+\infty, 0)$ together with k circles, connected together by p_1 regular intersections and p_2 tangencies, see Fig. 1. Here n, g_1 and g_2 are formal parameters, which can be evaluated at arbitrary complex values; however, it is natural to identify n with a number of *colors* one can assign to any of the closed loops of the diagram, so that the factor n^k correctly counts the total number of possible colorings of the diagram (assuming the external legs to carry a fixed color). The coefficient $a_{k,p,0}$ of the double generating function $G(n, g_1 = g, g_2 = 0)$ possesses the following interpretation: it is the number of alternating tangle diagrams with 2 external legs, k circles (i.e. $k+1$ connected components) and p crossings. The general coefficients do not possess such a clear knot-theoretic interpretation; however, they are needed to take into account the flyping equivalence (see [9,10]).

Fig. 1: Open curve and a circle with intersections (green dots) and tangencies (red dots).
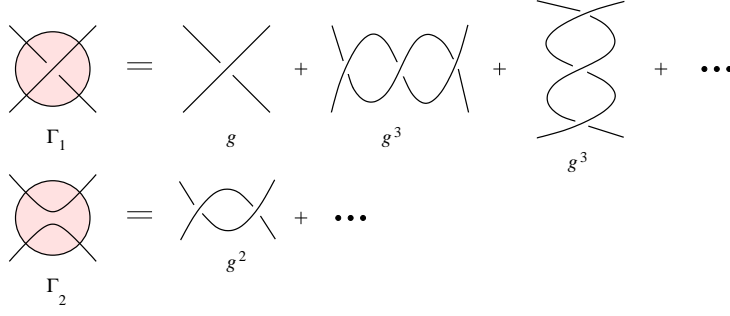
Fig. 2: Tangles of types 1 and 2 are distinguished by the two ways of connecting their external legs.

Next we define the generating functions of tangles Γ_1 and Γ_2 (see Fig. 2), which are necessary for the flyping equivalence. They are given by:

$$G = 1 + g_1 F_1 + g_2 F_2 \tag{2.2a}$$

$$\frac{\partial}{\partial g_2} F_1 = \frac{\partial}{\partial g_1} F_2 \tag{2.2b}$$

$$4F_1 = nG_1 + 2G_2 \tag{2.2c}$$

$$2F_2 = G_1 + (n+1)G_2 \tag{2.2d}$$

$$\Gamma_1 = G_1 \tag{2.2e}$$

$$\Gamma_2 = G_2 - G^2 \tag{2.2f}$$

via intermediate functions F_1, F_2, G_1, G_2. Note that inverting Eqs. $(2.2c, d)$ requires $n \neq 1, -2$. These special values of n will be investigated in detail in [10].

As in [4], we introduce an extra parameter to count edges of the diagram, according to the following definitions: $G(n, g_1, g_2, t) \equiv \frac{1}{t} G(n, g_1/t^2, g_2/t^2)$ and $\Gamma_i(n, g_1, g_2, t) \equiv \frac{1}{t^2} \Gamma_i(n, g_1/t^2, g_2/t^2)$.

The parameters t, g_1 and g_2 must then be chosen as a function of n and g according to the following *renormalization procedure* (see [10]):

$$1 = G(n, g_1(n, g), g_2(n, g), t(n, g)) \tag{2.3a}$$

$$g_1(n, g) = g(1 - 2H_2'(n, g)) \tag{2.3b}$$

$$g_2(n, g) = -g(H_1'(n, g) + V_2'(n, g)) \tag{2.3c}$$

where $H_1'(n, g)$, $H_2'(n, g)$ and $V_2'(n, g)$ are auxiliary quantities defined by:

$$H_2' \pm H_1' = \frac{(1 \mp g)(\Gamma_2 \pm \Gamma_1) \mp g}{1 + (1 \mp g)(\Gamma_2 \pm \Gamma_1) \mp g} \tag{2.4a}$$

$$H_2' + H_1' + nV_2 = \frac{(1 - g)(\Gamma_2 + (n+1)\Gamma_1) - g}{1 + (1 - g)(\Gamma_2 + (n+1)\Gamma_1) - g} \tag{2.4b}$$

3

These equations are independent only for $n \neq 0$, but have a smooth $n \to 0$ limit which is given in [4].

$\Gamma_1(n, g_1(n,g), g_2(n,g), t(n,g))$ and $\Gamma_2(n, g_1(n,g), g_2(n,g), t(n,g))$, once equations (2.3) are solved, are the desired generating functions for the number of prime alternating tangles of types 1 and 2 respectively [7] (see Fig. 2). The total number of tangles is given by $\Gamma_1 + 2\Gamma_2$. Similarly, one can define more general generating functions in the variables n, g_1 and g_2 which count tangles with more external legs; an explicit example will be given in Section 5.

3. The transfer matrices for alternating tangles

We now turn to the description of the two transfer matrices. The basic idea is common to both of them: starting from an initial state consisting of *all* external legs (i.e. two in the case under consideration), the system is time evolved through the addition of n intersections, until an empty final state is obtained.

Supposing the tangle diagram oriented from left to right, the first algorithm procedes by always evolving the uppermost vertex. We describe the details of this "single-step" algorithm in Section 3.1. The second algorithm, on the contrary, evolves all parts of the diagram simultaneously, adding one vertex to each of them in a given time step. In this way, the time can be defined as the geodesic distance from the pair of external legs. The details of this "geodesic" algorithm can be found in Section 3.2.

As in [4], we shall first concentrate on the enumeration of (prime, alternating) tangle *diagrams* with two external legs, which are related to the generating function $G(n, g = g_1, g_2 = 0)$ of Section 2. Adding tangencies, which is needed to take into account the flyping equivalence, will be discussed in Section 3.3, since it is an elementary extension of the algorithms.

Another minor modification of the algorithms will enable us to enumerate diagrams with more than two external legs; we shall develop this point in Section 3.4.

In both algorithms, the needs for CPU-time and memory increase exponentially with the system size p, though mercifully much more slowly than the number of knot diagrams actually being enumerated. As will become clear shortly, the single-step algorithm favors speed at the expense of memory consumption, while for the geodesic algorithm it is the other way around. However, since in practice both of these parameters are limiting factors for the maximally obtainable system size, it is a priori not clear which of the algorithms

4

performs best. We defer a detailed comparison to Section 4.3, and it turns out that the single-step algorithm comes out as the winner. Incidentally, even in the case of knots (one connected component), it performs slightly better than the algorithm described in [4].

3.1. The single-step algorithm

Let us briefly recall the working principle behind the knot enumeration algorithm presented in [4]. Reading the two-legged knot diagram from the first "ingoing" to the second "outgoing" leg, and calling at any instant the edge being read the "active line", there are two possibilities at each time step: 1) The active line is crossed by a line segment with edge labels that have not previously been encountered. We then add the new line segment to the current state. 2) The active line is identified with one of the endpoints of a line segment previously encountered. We then join the active line to that endpoint, wind around the line segment in question, and identify the new position of the active line with the opposite endpoint.
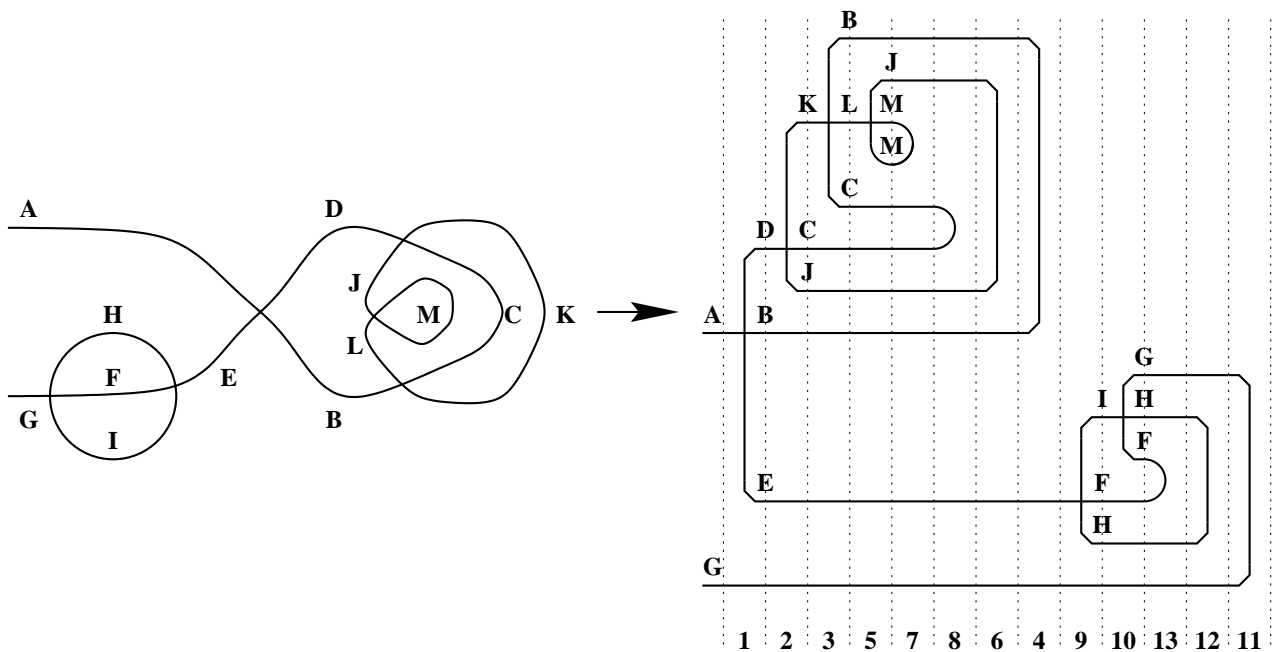
Fig. 3: Working principle of the single-step algorithm. a) A two-legged knot diagram with $p = 6$ intersections and $k = 3$ connected components. The edges are labelled from A to M. b) The same diagram in the time-slice representation. For reasons of clarity, the time slices are not drawn in chronological order.

5

The single-step algorithm can be viewed as a generalization of this principle. Let us, for the sake of illustration, consider the tangle diagram shown in Fig. 3. Since there is in general more than one connected component, clearly the concept of a unique "active line" no longer applies. Let us instead start from an initial state given by *both* external legs (edges A and G).

Moving along either of the edges A or G, a new line segment (DE resp. HI) is encountered. The question then arises which of these to process first. We resolve this ambiguity by stipulating that *in any given state, we evolve the line which at that instant is uppermost.*[1] At time $t = 1$, the edge A thus becomes B, and the new line segment DE is added. The edge D is now the new top line.

Analogously, at the instants $t = 2$ and $t = 3$, the top line (D resp. K) crosses a new line segment, which is then added to the current state. We can formalize this by stating the transformation rule shown in Fig. 4.1. This generalizes the corresponding rule of [4], except that the "active line" is now replaced by the uppermost line.

At time $t = 3$, the new top line carries the label B, which was however already produced by the transformation acting at $t = 1$. We therefore proceed, at $t = 4$, to the identification of the two "copies" of B, joining them through an arch. This is an example of the general transformation rule shown in Fig. 4.2. The addition of an arch means that the lines intermediate between the two instances of B (at positions $p = 1$ and q on Fig. 4.2) can henceforth not communicate with the lines at the exterior of the arch. These "trapped lines" must therefore eventually evolve to the empty state (vacuum), independently of the rest of the diagram. This observation has two implications: First, since both transformations conserve the parity (even/odd) of the number of lines, $p - q$ must be odd. Second, due to the above-mentioned rule that the current top line must always be treated first, the evolution of a possible set of "trapped lines" must take place at a later time. This means that when illustrating the sequence of moves on Fig. 3, we cannot *draw* the time-slices in chronological order. Note however, that the time ordering of the transformations is given by the time labels shown in the bottom of Fig. 3.

---

[1] With the optimization to be discussed in Sec. 4.2 we shall permit certain permutations of the lines. However, the line being evolved is in all cases the uppermost in the given *state*, though not necessarily in the corresponding time-slice representation.
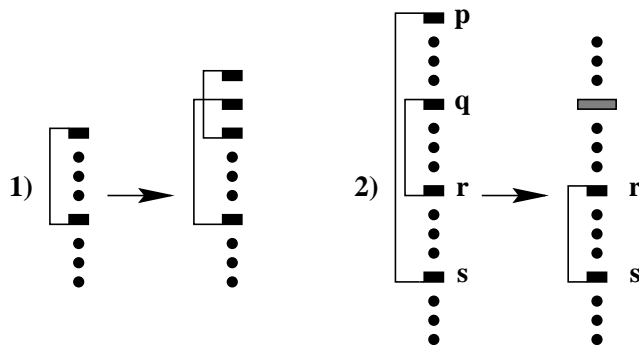
Fig. 4: The two types of transformations in the single-step algorithm. 1) Addition of a new line segment. 2) Identification of the top line (at position p) with another line (at position q), accompanied with the creation of a new block. Several remarks apply to the relative positions of p, q, r and s (see text).

The existence of a number of trapped lines is visualized on Fig. 4.2 by a *delimiter* (shown as a gray rectangle), which seperates the remaining lines into two *blocks*. Lines in different blocks cannot communicate, and must eventually evolve to the vacuum separately. In particular this means that the transformation 2) only applies when p and q belong to the same block. Conversely, q and r, and r and s may very well be separated by one or more delimiters (not shown). Also, although we have illustrated the case $r < s$, we may as well have $r > s$.

Of the thirteen transformations shown on Fig. 3, number 1, 2, 3, 5, 9, and 10 are of type 1, and the rest are of type 2. Clearly, the two types of transformations increase (resp. decrease) the number of lines by unity. Since the initial state consists of one line, the number of type 2 transformations must therefore exceed the number of type 1 transformations by one.

The purpose of the transfer matrix is not only to count the total number of tangle diagrams, but to do so for any fixed number of connected components. In particular, when performing a type 2 transformation, we need to know whether the points p and q were already connected though an arbitrary number of edges at an *earlier* time. On Fig. 4 we have represented this information by a number of lines on the left, connecting the points at a given instant into pairs. It may thus happen that on Fig. 4.2, $r = p$ and $s = q$. In this case, the type 2 transformation marks the completion of one connected component in the tangle diagram.

7
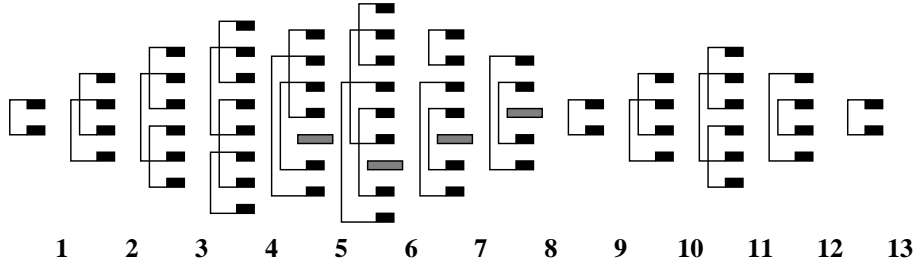
Fig. 5: Intermediate states produced by applying the single-step algorithm to the tangle diagram shown in Fig. 3.

We are now ready to define the set of *states* on which the transfer matrix acts. A state is defined by an even number of points (represented on Fig. 4 as black rectangles), connected into pairs by means of the edges encountered at previous times. In addition, the points are divided into $\ell + 1$ blocks by means of $\ell \geq 0$ delimiters. Note that points in different blocks can very well be connected, since any connection made beforehand persists after the addition of a delimiter.

On Fig. 5 we show the set of intermediate states corresponding to the time-slice representation of the tangle of Fig. 3. The initial state of a two-legged tangle is given by a pair of points (the exterior legs), implicitly connected at the point at infinity. It can be noted that the same state may occur at different instants of the transfer process. Also, any given state is not necessarily allowed at all instants.

After each type 2 transformation one may be able to simplify the set of delimiters. Namely, a delimiter may be eliminated if it is adjacent to another delimiter, or if it precedes the first point or succedes the last point of a state. On Fig. 5 we have implicitly assumed that such simplications have been carried out.

Finally, we must define the transfer matrix T which counts *all* tangle diagrams with $\tilde{p}$ vertices and k connected components. Its entries T_{ab}, where a and b are two basis states of the kind just defined, are 0 unless b is a descendant of a. An allowed state b is a descendant of a if it can be obtained via a transformation of one of the two types shown on Fig. 4 (for an arbitrary even $q \geq 2$ belonging to the same block as $p = 1$), followed by an arbitrary number of simplifications. T_{ab} is then the sum over all transformations from a to b of the corresponding weight: 1 or n depending on whether one closes a connected component or not (n can be either a given number, or a formal parameter, with a space of states enlarged by polynomials in n in the latter case). For the moment the simplications are just the elimination of superfluous delimiters. But we shall later (in Sec. 4.2) show that hitherto different states are equivalent by means of suitable transformations of the

8

blocks, and of the points within each block, such that a given state may be brought into a normal form. T then acts on the space of such normal forms. Apart from considerably reducing the dimension of the state space, these additional simplifications greatly enhance the efficiency of the algorithm.

As an example, we give in Appendix A the complete set of intermediate states with their corresponding weights for the counting of tangle diagrams up to four crossings.
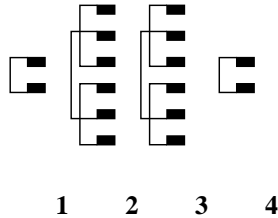
3.2. The geodesic algorithm

We now turn to the description of our second algorithm. Apart from providing a highly non-trivial check of our results, our motivation for developing this alternative algorithm was to try to limit the number of intermediate states and thus lower the memory needs of the program. We still define the initial state as the set of external legs, but we redefine the chronological order of the tangle diagram by taking the time coordinate to be the *geodesic distance to the set of external legs*.

Roughly speaking, in each time step we apply one of the transformations shown in Fig. 4 to *each* of the lines present in the state at that instant. However, in order to introduce a valid time ordering of the diagram this rough idea needs to be refined.
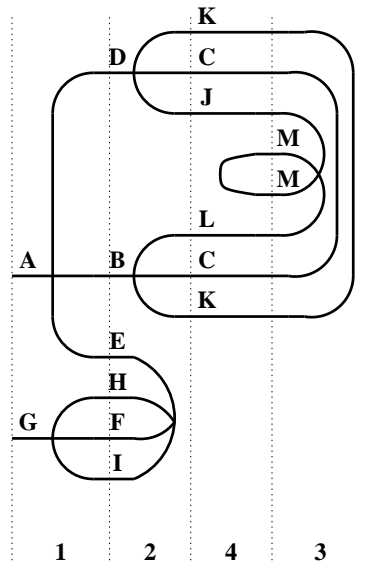
Fig. 6: The geodesic time-slice representation of the tangle diagram given in Fig. 3.

9

To progress, let us again consider the sample tangle diagram of Fig. 3. In Fig. 6 we show its new time-slice representation, this time using the above geodesic definition of time. At time $t = 1$ the edges A and G are both subject to the same transformation, in which three new edge labels (D, B, E resp. H, F, I) are encountered: as a short-hand notation we shall refer to this transformation as $1 \rightarrow 3$. It closely resembles the type 1 transformation in the single-step algorithm. When $t = 2$ the two upper edges (D and B) again undergo a $1 \rightarrow 3$ transformation, whereas the four lower edges (E, H, F, and I) annihilate at a common vertex: this is the $4 \rightarrow 0$ transformation. At the instant $t = 3$, it is recognized that two edge pairs (K and C) created at $t = 2$ carry the same label and thus must be identified. This transformation is reminiscent of the type 2 transformation in the single-step algorithm, and we shall here tag it $2 \rightarrow 0$. At the same time, the two edges J and L cross so as to become a new pair of edges, which are incidentally both labelled M. This is yet another transformation, the $2 \rightarrow 2$.

Fig. 7: Intermediate states used by the geodesic algorithm.

The intermediate states produced by this time-slice representation of this example are listed in Fig. 7. When comparing with the single-step algorithm (see Fig. 5) we note a considerable simplification.

Turning now to the general case, we see that apart from the $2 \rightarrow 0$ move, the transformations discussed above simply express the various ways of "time ordering" a tetravalent vertex, i.e. to assign the label t to at least one of its incident edges, and the label $t + 1$ to the remaining edges. The possibility $0 \rightarrow 4$ is excluded, as it would lead to the creation of disconnected diagrams. This leaves us with the transformations $4 \rightarrow 0$, $3 \rightarrow 1$, $2 \rightarrow 2$ and $1 \rightarrow 3$. But due to the planarity of the diagrams, one also needs to take into account that some of these transformations exist in several variants. For example, the "tadpole" labelled M on Fig. 6 is situated to the left of its adjacent vertex; however, a different diagram exists in which it is situated to the right. One must therefore accept that the transformation $2 \rightarrow 2$ comes in (at least) two guises: in the first, the outgoing edges bend backwards to the left, in the other they continue to the right.
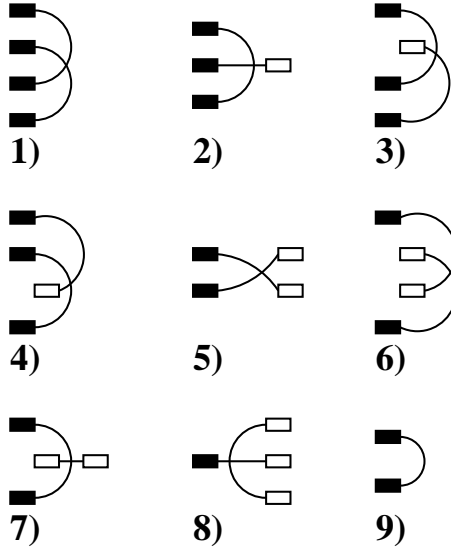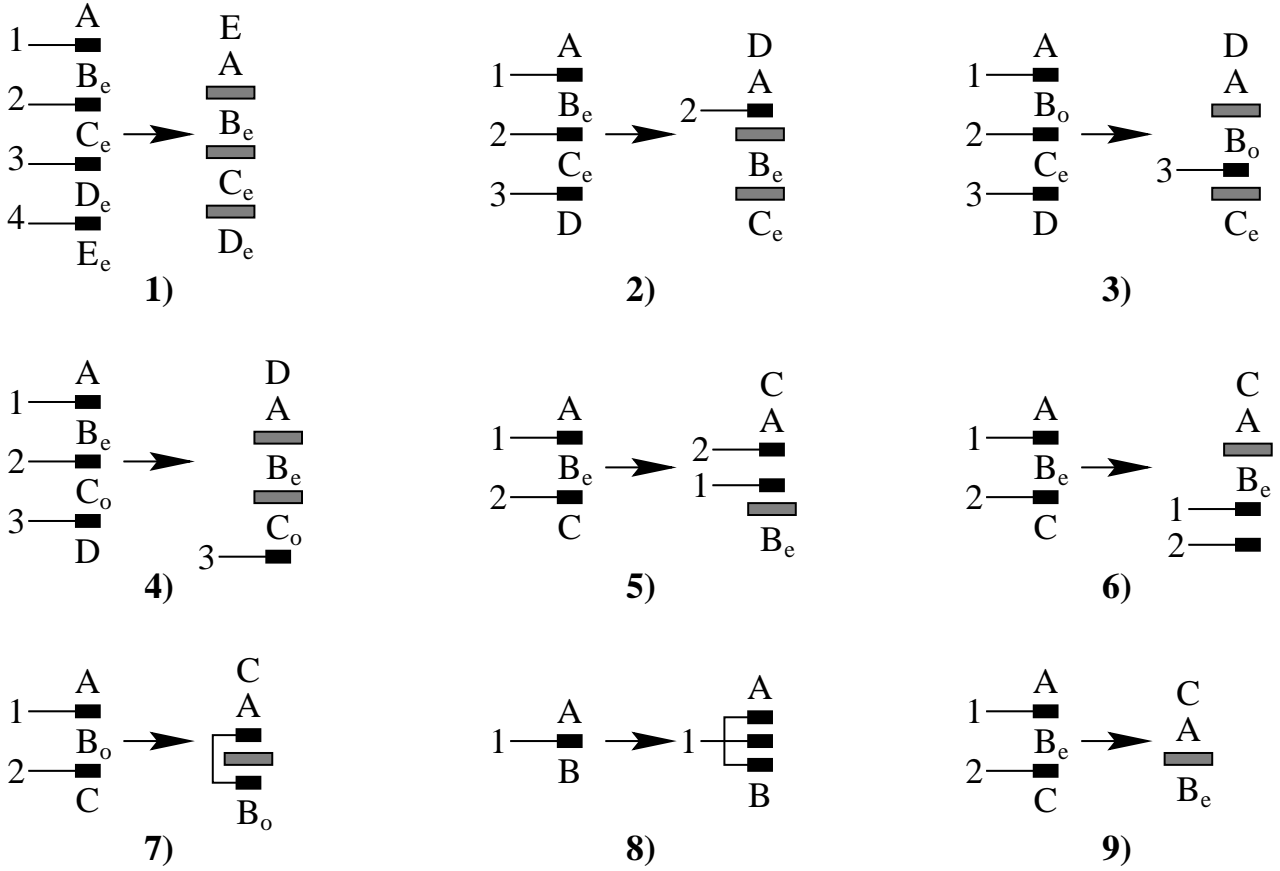
Fig. 8: Schematic transformation rules for the geodesic transfer matrix.

In Fig. 8 we show schematically the complete set of transformation rules. The black rectangles represent points at time t, and the white ones points at $t + 1$. The solid lines indicate the action of the transfer matrix at time t. The first eight transformations are simply the topologically inequivalent ways of presenting a tetravalent vertex with at least one point labelled by t. In particular we note that the transformations of type $2 \to 2$ and $3 \to 1$ each occur in three different variants. The more exotic possibilities 3, 4 (resp. 5) start contributing to tangle diagrams with at least 4 (resp. 5) crossings. Finally, the ninth transformation is simply the $2 \to 0$.

We still need to transcribe these rules in terms of the states previously defined. In general, a given transformation leads to the creation of several new enclosed regions (blocks), and to represent the latter in terms of delimiters one needs to make use of the fact that cyclically permuting the points within a given block yields a topologically equivalent state (we shall come back to this point later, in Sec. 4.2). Also, since each block must evolve separately to the vacuum there are various parity constraints on the positions of the points entering a given transformation. By convention, we shall use capital letters to designate (possibly empty) blocks of points. Subscripts e and o indicate that the number of points must be even (resp. odd). Blocks with no subscript may have any parity: they are however subject to the global constraint that the total number of points must be even. Represented in this way, the exact transformation rules are given in Fig. 9.

Just like in the single-step algorithm, a transformation may be followed by an arbitrary number of simplifications (see Sec. 3.1).

11

Fig. 9: Exact tranformation rules for the geodesic transfer matrix.

3.3. Tangencies

Until now we have been discussing the enumeration of tangle diagrams in which every vertex represents a crossing. However, to account for the flype equivalence we need to enumerate more general diagrams with p_1 intersections and p_2 tangencies, as discussed in Section 2. Fortunately, this is a very simple extension of either of our algorithms.

Let us for simplicity consider the case of the single-step algorithm. Adding a tangency rather than an intersection is obtained by modifying the transformation if Fig. 4.1, so that the two points added at time $t + 1$ are both immediately above (resp. immediately below) the uppermost point at time t. Calling these variants respectively transformation 1a and 1b, a knot diagram with intersections and tangencies is then generated by acting on the initial state with a sequence of transformations 1, 1a, 1b and 2.

We also need to add to the characterization of each state a variable that, at any given time, specifies how many tangency transformations (type 1a or 1b) were used prior to that instant. The desired diagrams are then generated by sequences of p_1 transformations

12

of type 1, p_2 of type 1a or 1b, and $p_1 + p_2 + 1$ transformations of type 2, so that no intermediate state is empty.

Omitting the details, we notice that it is equally straightforward to include tangencies in the geodesic algorithm by obvious modifications of the eight first transformations of Fig. 8.

3.4. More external legs

Another extension of our algorithms consists in the enumeration of diagrams with 2ℓ external legs, $\ell > 1$. To this end we simply start from an appropriate initial state comprising ℓ line segments, instead of just one, and we demand that the total number of type 2 transformations exceed the total number of type 1 (i.e. 1, 1a, or 1b) transformations by ℓ.

For $\ell > 1$, such diagrams come in several types, corresponding to the number of ways of pairwise connecting the set of external legs at infinity. More precisely, given an ordered set of 2ℓ points $X_\ell \equiv \{x_1, x_2, \ldots, x_{2\ell}\}$, the number of types equals the number of ways to divide the set X_ℓ into pairs, considered up to the action of the dihedral group $D_{2\ell}$ on X_ℓ.[2] In particular, there are two types of (four-legged) tangles (see Fig. 2), and five types of tangles with $2\ell = 6$ external legs (see Section 5). The general integer sequence $1, 2, 5, 17, 79, \ldots$ thus defined is discussed in [11].

4. Implementational details

Although both of the algorithms described in the previous section are operational (as the reader may verify by studying Appendix A), we still need to give various details relative to their implementations on a computer. In particular, it is not clear how states of the type shown in Fig. 5 may be conveniently represented and manipulated. We shall address this question in Section 4.1. Another important observation is that states which until now have appeared to be different are in fact topologically equivalent. We shall discuss this point in Section 4.2 and demonstrate how it can be used to improve the efficiency of both algorithms. Finally, we compare the performances of the two different algorithms (single-step and geodesic) in Section 4.3.

---

[2] This also has a group-theoretic interpretation, in terms of number of $O(n) \times D_{2\ell}$-invariants in the tensor product of 2ℓ fundamental representations of $O(n)$, for generic n.

4.1. Representation of the states

In order to render the information contained in states of the type shown in Fig. 5 machine recognizable we shall represent each of them by an ordered list of non-negative integers. The length of the list representing a given state equals the number of points in the state plus the number of delimiters, and the order of its elements is given simply by reading the state from top to bottom. Each delimiter is represented by the digit zero. The other points each correspond to a positive integer, with the convention that two points are connected if and only if they are represented by the same integer. Clearly, this convention is not unique: for instance, $(1, 2, 0, 1, 2)$ and $(13, 4, 0, 13, 4)$ both describe the same state. To get rid of this ambiguity we shall stipulate that each consecutive digit, starting from the left, be chosen as small as possible, consistent with the above rules. Thus, $(1, 2, 0, 1, 2)$ is the unique normal form of our sample state.

The sequence of states shown in Fig. 5 can then be transcribed as follows:

$$(1, 1) \rightarrow (1, 2, 1, 2) \rightarrow (1, 2, 1, 3, 2, 3) \rightarrow (1, 2, 1, 3, 2, 4, 3, 4) \rightarrow (1, 2, 3, 1, 0, 3, 2)$$
$$\rightarrow (1, 2, 1, 3, 4, 2, 0, 4, 3) \rightarrow (1, 1, 2, 3, 0, 3, 2) \rightarrow (1, 2, 0, 2, 1) \rightarrow (1, 1)$$
$$\rightarrow (1, 2, 1, 2) \rightarrow (1, 2, 1, 3, 2, 3) \rightarrow (1, 2, 2, 1) \rightarrow (1, 1).$$

At a given stage in the transfer process we need to run through the states present at time t, apply the transformation rules described in Section 3.1–3.2, and produce the set of descendant states (the states at time $t + 1$) with their respective weight. The first time a given descendant state is produced, it must be inserted in a suitable data structure along with is weight. If subsequently the same state is produced again as a descendant of another parent state, rather than inserting it again we need to retrieve it in the data structure and update its weight. In order for the algorithm to be efficient, the operations of insertion and retrieval must be accomplished in constant time (i.e. in a time that does not depend on the number of states accomodated by the data structure).

These demands are fulfilled by a standard data structure known as a *hash table* [12]. It relies on the fact that to each state i we can assign a unique integer $k_i \in \mathbb{Z}_+$ (the hash key), and devise a function $f : \mathbb{Z}_+ \rightarrow \{0, 1, 2, \ldots, P - 1\}$ (the hash function) that distributes the set of k_i's more-or-less uniformly on the set $\{0, 1, 2, \ldots, P - 1\}$. By inserting the states i into an array of noded lists indexed by $f(k_i)$, we can retrieve any given state in a time proportional to the mean length of one of the pointer lists, $t \propto N/P$, where N is the total

14

number of entries. In practice we choose P to be a large prime such that $N/P \sim 10$, and we use the hash function $f(k) = k \bmod P$.

A convenient key k_i can be defined by concatenating the list of "digits" entering the normal form of the state i into one large integer. To find the minimum number of bits required to store one digit, we remark that for the counting of tangles with ℓ intersections the digits are all $\leq \ell + 1$. In the case at hand this means that we need to use at least five bits per digit; in practice we have however chosen to use eight bits, in order to profit from standard routines for handling character strings.

4.2. Equivalences between states

As has already been mentioned, it is true for either of the two tangle enumeration algorithms that some of the states generated at a given stage in the transfer process are topologically equivalent. Clearly, it is of the utmost interest to factor out as many topological equivalences as possible from the state space, since the memory demands as well as the time consumption of the algorithm are roughly proportional to the number of states being treated.

A first such equivalence is due to the fact that any two different blocks of points must evolve separately to the vacuum, without any mutual interaction. The relative position of the blocks is thus immaterial. The standard version of either algorithm (say, version 1) can thus be ameliorated by introducing a standard order among the blocks before inserting a given state in the hash table (version 2). We have done so by simply sorting the blocks according to their size. In the special case of the single-step algorithm it is advantageous to place the smallest blocks at the top of the state, since such blocks will then be evolved to the vacuum before touching any other block. The small block being eliminated, the remainder of the state will be smaller and can thus be processed more expeditiously. For the geodesic algorithm, the choice betwen ascending and descending ordering is irrelevant.

We take the convention of not changing the relative order of two equally sized blocks.[3] After the permutation of the blocks, the representation of the state in terms of a list of integers is brought back to its normal form (see Sec. 4.1).

---

[3] Inspecting by hand some modestly sized systems reveals that changing the order of equally sized blocks will only lead to a very small further gain. We have nevertheless made various attempts of imposing a more unique way of arranging the blocks, but since such transformations tend to break down a certain regularity in the connectivities which is imposed by the type 1 transformation, these attempts actually resulted in a slight *increase* in the number of states.

p	version 1	version 2	version 3
2	4	4	4
3	7	7	6
4	24	16	14
5	67	45	24
6	226	110	49
7	735	313	106
8	2573	804	209
9	9340	2160	479
10	32790	6345	1078
11	128794	17074	2382
12	468757	45858	5929
13	1933350	127751	13992

Tab. 1: Maximal number of intermediate states in the transfer process for three different versions (see text) of the single-step algorithm for tangle diagrams with p self-intersections and no tangencies.

In Table 1 we illustrate the resulting decrease in the number of states inserted in the hash table. It seems clear that not only is the number of states much smaller, but it even grows with a smaller exponent.

Second, the states are equivalent upon cyclic rotations (eventually combined with a reflection) of the points within any given block. Since, once again, the blocks are independent, these dihedral transformations can be performed independently within each block. The ultimate way of implementing this equivalence would be the following: before inserting a state in the hash table, subject it to all possible dihedral transformations, and check whether any of the transformed states is already present in the table. Unfortunately, the number of transformations increases faster than exponentially with the size of the state, and this exhaustive search would quickly end up usurping the majority of the CPU time.

We have therefore opted for a less perfect but much faster alternative (version 3).[4] Having sorted the blocks according to their size, we consider in turn all possible dihedral transformations on the points in the first block, keeping fixed the positions of the points in the other blocks. After each transformation we bring the integer representation of the state

---

[4] Comparing with the exhaustive method applied to some modestly sized systems shows that, once again, the number of topological equivalences not detected by the "approximate" method is negligible when compared to the number of states which are in fact topologically distinct.

into its normal form. We then identify (one of) the normal form(s) which lexicographically precedes all the others, and lock the points of the first block into their corresponding positions. Leaving the first block locked, we procede to apply the same procedure to the second block. We continue this way until all blocks have been locked, and only then the resulting representation of the state is inserted into the hash table.

The gain of version 3 over version 2 is comparable to the gain of version 2 over version 1, as witnessed by Table 1. In the following we shall therefore exclusively understand version 3 when referring to any one of the two algorithms (single-step or geodesic).

4.3. Comparing the two algorithms

A first striking difference between the single-step and the geodesic algorithm can be observed by comparing how their respective number of intermediate states (and thus the memory needs) evolve as a function of the "time" defined by the transfer process.
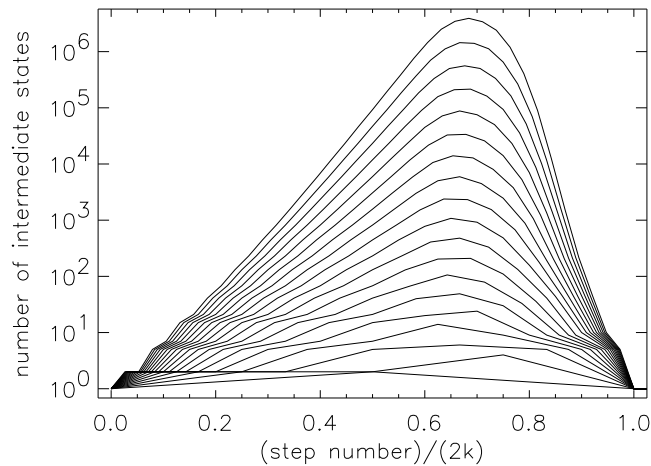
Fig. 10: Memory profile of the single-step algorithm (version 3, cf. Sec. 4.2). The curves represent knot diagrams with $p = 1, 2, \ldots, 19$ crossings and no tangencies.

In both cases, the number of states grows exponentially in the beginning, decreases exponentially towards the end, and reaches a maximum somewhere in between. However, for the single-step algorithm this maximum is reached at roughly $2T/3$ (where T is the total number of time steps), whereas for the geodesic algorithm the maximum is situated around $T/4$. The reason for this difference is that the geodesic algorithm will produce the majority of its states by applying the $1 \rightarrow 3$ rule as often as possible in the beginning of the process.

17
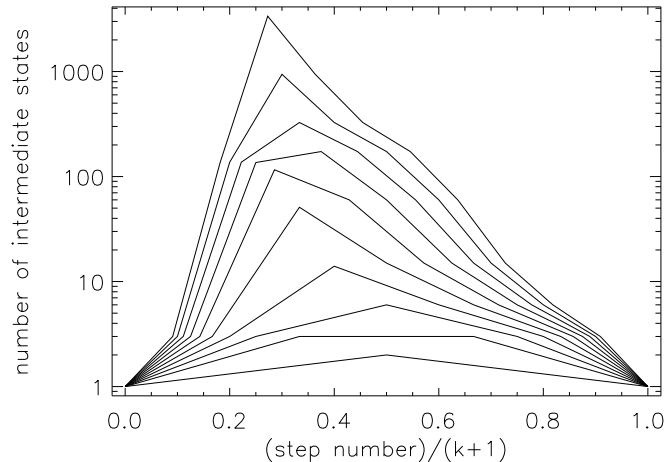
Fig. 11: Memory profile of the geodesic algorithm (version 2, cf. Sec. 4.2). The curves represent knot diagrams with $p = 1, 2, \ldots, 10$ crossings and no tangencies.

p	version 1	version 2	version 3
2	3	3	3
3	6	6	6
4	14	14	12
5	60	51	37
6	141	116	86
7	207	173	126
8	396	327	238
9	1308	941	544
10	5300	3367	1701

Tab. 2: Maximal number of intermediate states in the transfer process for three different versions (see Sec. 4.2) of the geodesic algorithm for tangle diagrams with p self-intersections and no tangencies.

To estimate the actual memory needs of the algorithms, it is instructive to compare the maximal number of intermediate states for the three different versions defined in Sec. 4.2. For the single-step algorithm the data were given in Tab. 1; we show the corresponding numbers for the geodesic algorithm in Tab. 2. As expected, version 1 of the geodesic algorithm employs considerably fewer states than version 1 of the single-step algorithm. However, quite surprisingly, the ameliorations implied by version 2 and version 3 lead to an enormous gain in the single-step case, but only a modest one in the geodesic case.

18

Thus, in version 3 the asymptotic growth of the number of states is significantly slower in the single-step algorithm than in the geodesic one, even though the latter was explicitly designed to use fewer states! Although a qualitative explanation of this phenomenon can be given by inquiring into the structure of a typical state we refrain from doing this here. Rather, let us simply accept the efficiency of the single-step algorithm as a remarkable fact.

Even when discarding the issue of memory, the geodesic algorithm has a serious drawback compared with its single-step counterpart as far as time consumption is concerned. Namely, the single-step algorithm processes each state in a time that grows roughly linearly with its size, whereas for the geodesic algorithm this time grows exponentially. To see this, consider the intermediate state which is obtained from the initial state by performing p transformations of type $1 \to 3$. To turn this state into tangle diagrams with exactly p crossings, one needs to complete it with $p + 1$ transformation of type $2 \to 0$. Supposing p chosen so that the intermediate state has a complete number of time slices, a total of c_{p+1} diagrams will be recursively generated, where $c_k = \frac{(2k)!}{k!(k+1)!}$ are the Catalan numbers. The geodesic algorithm will therefore (asymptotically) spend the majority of the CPU time closing up this "maximally opened state".

We have therefore used the geodesic algorithm as a highly non-trivial check of our numerical results, but the data for large system sizes are generated exclusively by the single-step algorithm.

To conclude this section, let us briefly discuss the time complexity of our best algorithm (single-step, version 3). Based on the data in Tab. 1, we infer that both time and memory needs grow asymptotically as $\sim \kappa^p$, with $\kappa \approx 2.7 \pm 0.2$.

5. Numerical results

We now present the numerical results that we obtained using the single-step algorithm (version 3). Due to the enormous amount of data gathered we shall only give the main results.

The first data are obtained by running a program that implements the single-step algorithm without any tangencies. This corresponds to the generating function $G(n, g_1 = g, g_2 = 0)$ in the notation of Section 2. Its coefficients $a_{k,p,0}$ are given in Table 3 up to $p = 19$. The computation took a few hours on a 1 GHz single-processor work station with 1 GByte of memory.

k\p	0	1	2	3	4	5	6	7	8	9
0	1									
1	2									
2	8	1								
3	42	12								
4	260	114	4							
5	1796	1030	90							
6	13396	9290	1349	22						
7	105706	84840	17220	728						
8	870772	787082	203568	14884	140					
9	7420836	7415814	2312094	244908	6120					
10	65004584	70867212	25691670	3575045	158354	969				
11	582521748	685839770	282000444	48517524	3185314	52668				
12	5320936416	6712285600	3074136464	628013796	55273668	1647728	7084			
13	49402687392	66349573368	33387698708	7871666088	871779428	39142116	460460			
14	465189744448	661680191832	361969672904	96451145091	12876308613	786444610	16890227	53820		
15	4434492302426	6651030871168	3921901043440	1162484964230	181430681094	14126467392	462455640	4071600		
16	42731740126228	67329662060890	42499598861832	13840075278704	2468480436152	234358127880	10552931952	171277860	420732	
17	415736458808868	685953949494774	460831546801414	163246693686684	32699872694298	3666111325052	212581611050	5308497112	36312408	
18	4079436831493480	7028941367108708	5001468564165262	1911737961254907	424232095742826	54835331971380	3912429396360	135564649071	1722788176	3362260
19	40338413922226212	72403769391718890	54341248085414380	22262254374655710	5413174461572394	791922013806504	67266181855770	3025712334552	59605106568	326023280

Tab. 3: Table of the number of alternating tangle diagrams with 2 external legs.

Let us first note that there are various quantities which can be extracted from this table and which are known exactly in an independent way. They provide a number of non-trivial checks. Let us define the number $a_p(n)$ of diagrams at fixed number of colors n

$$a_p(n) = \sum_{k=0}^{\infty} a_{k,p,0} n^k \tag{5.1}$$

The simplest choice is to set $n = 1$, that is to consider the sum of each row of the table. This series of numbers is known exactly (see [13] for a purely combinatorial argument, and [14] for a field theoretic one)

$$a_p(1) = 2\frac{(2p)!}{p!(p+2)!}3^p \tag{5.2}$$

and the corresponding generating function is

$$G(1, g, 0) = \frac{1}{3}A(4 - A) \tag{5.3a}$$

$$A = \frac{1 - \sqrt{1 - 12g}}{6g} \tag{5.3b}$$

It is perhaps less well known that for $n = 2$, one also has an exact expression, in terms of elliptic integrals [15]:

$$G(2, g, 0) = \frac{1}{g^2}\left(\frac{g}{2} - \frac{1}{8}\frac{k}{(1 + k)^2}\right) \tag{5.4a}$$

$$g = \frac{E(k) - (1 - k)K(k)}{2\pi(1 + k)} \tag{5.4b}$$

where $K(k)$ and $E(k)$ are the complete elliptic integrals of the first and second kinds. We note that the generating function is non-algebraic, and it is not known how to find it by direct combinatorial arguments.

There exists a similar, although more complicated, formula for the case $n = -2$ which will be presented elsewhere [10].

One can also find expressions for the last non-zero element of each row, which formally corresponds to $n \to \infty$ (with $x \equiv ng^2$ fixed). However there is a parity effect which forces us to redefine separately odd and even generating functions:

$$H_{\text{even}}(x) = \sum_{k=0}^{\infty} a_{k,2k,0}\, x^k \qquad (5.5a)$$

$$H_{\text{odd}}(x) = \sum_{k=0}^{\infty} a_{k,2k+1,0}\, x^k \qquad (5.5b)$$
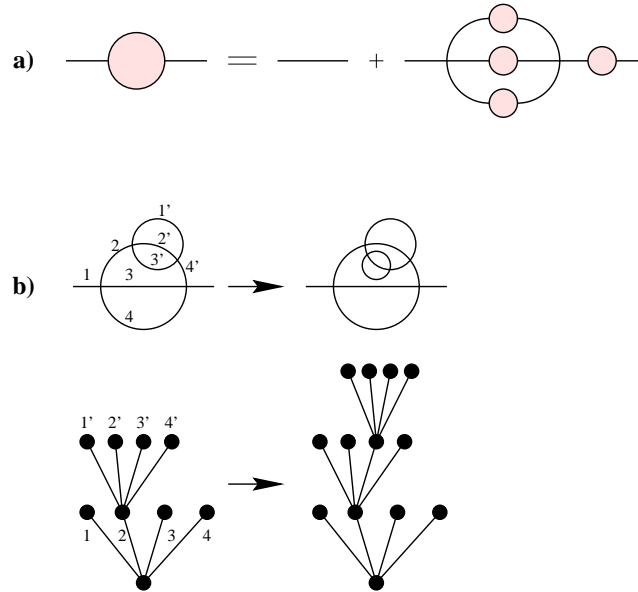
Fig. 12: a) Equation satisfied by $H_{\text{even}}(x)$. b) Recursive definition of a circle diagram and its interpretation in terms of a rooted tree.

For the even case, a general diagram has the form of successive insertions of circles in the bare propagator, which leads to the equation, depicted on Fig. 12 a),

$$H_{\text{even}} = 1 + xH_{\text{even}}^4 \qquad (5.6)$$

21

This can be described more explicitly in terms of rooted trees. Each insertion of a circle requires two additional intersections, and it leads to the creation of four new edges in which new circles can be inserted. On Fig. 12 b) we have labelled two successive generations of edges as $\{1, 2, 3, 4\}$ and $\{1', 2', 3', 4'\}$ respectively. Clearly, this reduces the problem to that of enumerating rooted trees in which each node (resp. the root) can have degree 1 or 5 (resp. 0 or 4). This is a simple example of a rather broad class of rooted trees discussed by Takács [16].

From Eq. (5.6) we infer that

$$a_{k,2k,0} = \frac{(4k)!}{(3k+1)!\,k!} \tag{5.7}$$

The proof of the formula for $H_{\mathrm{odd}}(x)$ is left as an exercize to the reader:

$$H_{\mathrm{odd}} = 2\frac{\mathrm{d}}{\mathrm{d}x}(xH_{\mathrm{even}}^3) \tag{5.8}$$

We infer that

$$a_{k,2k+1,0} = 2\frac{(4k+2)!}{(3k+2)!\,k!} \tag{5.9}$$

Finally, the first column in Table 3 reproduces the knot diagrams discussed in [4], of course.

Next we want to deduce some properties of the asymptotic behavior of these series from the numerical data. The first quantity one can extract is the "bulk entropy" of alternating tangles and links.[5] At fixed n it is defined by the leading exponential behavior of $a_p(n) \sim \mathrm{e}^{\hat{s}(n)p}$:

$$\hat{s}(n) = \lim_{p\to\infty} \frac{\log a_p(n)}{p} \tag{5.10}$$

It would however be more natural to consider alternating links/tangles at fixed number of connected components. This requires making an appropriate scaling ansatz for the coefficients $a_{k,p,0}$, which turns out to be

$$\log a_{k,p,0} \overset{k,p\to\infty}{\sim} p\,s(k/p) \tag{5.11}$$

where $s(x)$ is the bulk entropy at fixed ratio x of the number of connected components by the number of crossings. It is clear from Eq. (5.1) that the two entropies defined above are

---

[5] The bulk behavior should be independent of the number of external legs, and in particular be the same for links and tangles.

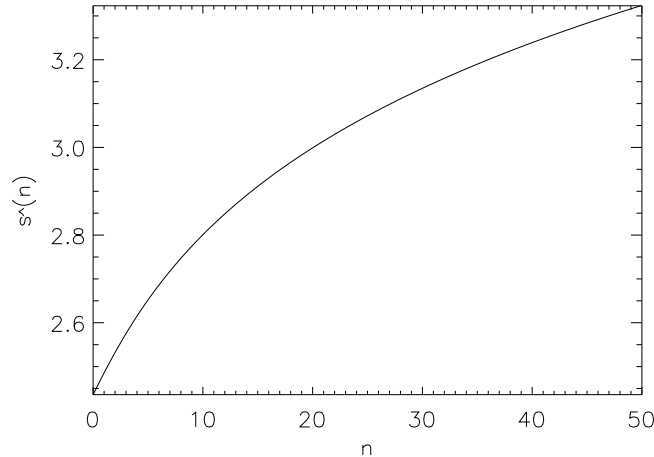related to each other by a Legendre transform; namely, if one defines the *average* ratio x at fixed n:

$$x(n) = \frac{\mathrm{d}}{\mathrm{d}\log n}\hat{s}(n) = \left\langle \frac{k}{n} \right\rangle \qquad (5.12)$$

then the following relation holds:

$$s(x(n)) = \hat{s}(n) - x(n)\log n \qquad (5.13)$$

so that we also have the dual equation of (5.12)

$$-\log n = \frac{\mathrm{d}}{\mathrm{d}x}s(x(n)) \qquad (5.14)$$

Fig. 13: The bulk entropy $\hat{s}(n)$.

On Fig. 13 the behavior of $\hat{s}(n)$ is shown for $n \in [0, \infty]$. The various exact solutions mentioned above correspond to the following known values of $\hat{s}(n)$:

$$\hat{s}(1) = \log 12$$

$$\hat{s}(2) = \log 4\pi$$

$$\hat{s}(n) \overset{n \to \infty}{=} \frac{1}{2}\log n + \log\frac{16}{3\sqrt{3}} + o(1)$$

In [4], the following numerical value was given: $\exp \hat{s}(0) \approx 11.42$, which is confirmed here.

23
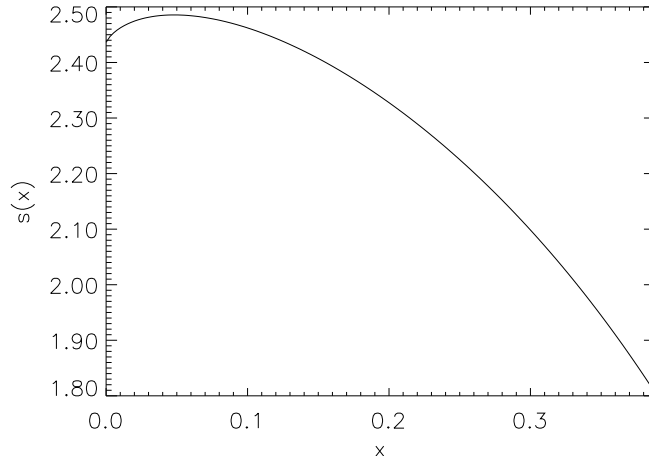
Fig. 14: The bulk entropy $s(x)$.

Even more interesting is the curve $s(x)$ shown on Fig. 14 for $x \in [0, 1/2]$. It displays a clear maximum at a value which is nothing but $x(1)$, cf Eq. (5.14). Numerically we find:

$$x(1) = 0.0481 \pm 0.0001 \tag{5.16}$$

This number has the following significance: at fixed number of crossings p, a typical tangle/link diagram will have $0.0481 \cdots \times p$ connected components when p goes to infinity. Note that this number is extremely small: any average made over (equally weighted) alternating link diagrams will be dominated by objects with few connected components.

Let us note that the bulk quantities *are affected* by the various renormalizations of Eq. (2.3), i.e. restriction to 2PI diagrams and inclusion of the flype equivalence. However, it is expected that the qualitative properties (and in particular the maximum of the entropy for a very small value of x) are unchanged. For example, if one considers 2PI diagrams (which corresponds to the counting of reduced prime alternating link/tangle diagrams), one finds a maximum at $x_2(1) \approx 0.033$ instead.

The discussion of the exponent associated to the subdominant power-law behavior of the series $a_p(n)$ (or, equivalently, $a_{k,p,0}$) is much more involved. We define the critical exponent

$$\alpha(n) = \lim_{p \to \infty} \frac{-\log a_p(n) + p \, \hat{s}(n)}{\log p} \tag{5.17}$$

Let us first recall the conjecture made in [9], which relies on several hypotheses: a) the asymptotic behavior of $a_p(n)$ is related to a singularity of the corresponding generating

function $G(n, g, 0)$ which has the physical meaning of singularity of 2D quantum gravity, i.e. large link diagrams behave as continuum random surfaces for which conformal field theory techniques apply (KPZ formula [17]); b) the model describing link diagrams with n colors is in the same universality class as the usual $O(n)$ model of dense loops [18], which relies on the assumption that there is no phase transition in the generalized $O(n)$ matrix model. For $|n| < 2$, $n = -2\cos(\pi\nu)$ $(0 < \nu < 1)$, this implies that

$$\alpha(n = -2\cos(\pi\nu)) = 1 + 1/\nu \tag{5.18}$$

Let us now discuss separately various regions of n and the corresponding numerical analysis.
• For $n < 0$, a difficulty arises in that coefficients $a_p(n)$ do not have a fixed sign. This implies in particular that the dominant singularity of the generating function $G(n, g, 0)$ is not necessarily on the real positive axis, as would be implied by hypothesis a) above. Numerically it seems that pairs of complex conjugated singularities do occur and become dominant in a large region of n which includes at least part of the interval $n \in [-2, 0[$, thus invalidating conjecture (5.18) in this region. The analysis of such behavior is fairly involved and we leave it to future work.
• $0 \leq n < 1$: at $n = 0$ it was suggested in [4] that even though conjecture (5.18) is correct $(\alpha(0) = 3)$, there might be a logarithmic correction which spoils the asymptotic behavior of the coefficients. For n small, we expect several singularities extremely close to the dominant singularity making any analysis difficult. Estimates of the critical exponent do not contradict (5.18), but they have very low accuracy; for example,

$$n = \frac{\sqrt{5}-1}{2} \qquad \nu = 3/5 \qquad \alpha_{\text{conj}} = \frac{8}{3} \qquad \alpha_{\text{num}} = 2.6 \pm 0.1 \tag{5.19}$$

• $1 \leq n \leq 2$: we can first extract from the exact solutions (Eqs. (5.2), (5.3) and (5.4)) the asymptotics

$$a_p(1) \sim 12^p p^{-5/2} \text{cst} \tag{5.20.1}$$

$$a_p(2) \sim (4\pi)^p p^{-2}(\log p)^{-2} \text{cst} \tag{5.20.2}$$

They are of course compatible with (5.18); however we note a logarithmic correction in (5.20.2) which comes from inverting the singularity of Eq. (5.4): $g - g_c \sim (k - k_c)\log(k - k_c)$. At this point it becomes clear that in order to remove the $(\log p)^{-2}$ factor, one just needs to perform an appropriate functional inversion on the generating series $G(2, g, 0)$. Applying

the same procedure to the numerical data of $G(n, g, 0)$ for $1 \leq n \leq 2$, one can then use standard convergence acceleration methods and obtain precise estimates of the critical exponent. They are in good agreement with (5.18); for example,

$$n = \sqrt{2} \qquad \nu = 3/4 \qquad \alpha_{\text{conj}} = \frac{7}{3} \qquad \alpha_{\text{num}} = 2.34 \pm 0.01 \qquad (5.21)$$

• $n > 2$: let us first recall that we have found exact expressions at $n \to \infty$ for odd and even coefficients separately (Eqs. (5.7) and (5.9)). Asymptotically,

$$a_{k,2k,0} \sim \left(\frac{256}{27} \right)^k k^{-3/2} \text{cst} \qquad (5.22a)$$

$$a_{k,2k+1,0} \sim \left(\frac{256}{27} \right)^k k^{-1/2} \text{cst} \qquad (5.22b)$$

i.e. the bulk terms are identical but the critical exponents are different. This can be understood easily since in the odd case there is one "defect" in the sequence of circles which corresponds to marking one connected component, that is multiplying by k (cf the differentiation in Eq. (5.8)).

Numerically, it is clear that for all $n > 2$ odd and even series behave differently. However once cannot perform any serious analysis on these series since they are too short. It may be that the exponents of Eq. (5.22) are preserved for any $n > 2$, or finite values of n might smooth the difference between odd and even series; the data we possess are unconclusive on this issue.

Let us end this analysis by noting that contrary to the bulk terms, critical exponents are expected to be *independent* of the various renormalizations of Eq. (2.3), due to universality arguments.

We now turn to the data obtained by inclusion of tangencies. For reasons of conciseness, we here refrain from displaying the three-dimensional array of coefficients a_{k,p_1,p_2}; these are electronically available from the authors upon request. Even the final results are fairly cumbersome to treat and display, so that we only show the results for the number of prime alternating tangles up to $p = 15$ (even though they can be easily obtained for p up to 18 or 19, as in [4], on a work station, and probably a bit further using larger computers).

These data satisfy once more various non-trivial checks, including the comparison with the table in the appendix of [5] (for $n = 1$), of the Tables 1 and 2 in [7] (for $n = 2$), and Table 3 of [4] (for $n = 0$).

26

	Γ_1							Γ_2						
$p \backslash k$	0	1	2	3	4	5	6	0	1	2	3	4	5	6
1	1							0						
2	0							1						
3	2							1						
4	2							3	1					
5	6	3						9	1					
6	30	2						21	11	1				
7	62	40	2					101	32	1				
8	382	106	2					346	153	24	1			
9	1338	548	83	2				1576	747	68	1			
10	6216	2968	194	2				7040	3162	562	43	1		
11	29656	11966	2160	124	2			31556	17188	2671	121	1		
12	131316	71422	9554	316	2			153916	80490	15295	1484	69	1	
13	669138	328376	58985	5189	184	2		724758	425381	87865	6991	194	1	
14	3156172	1796974	347038	22454	478	2		3610768	2176099	471620	52231	3280	103	1
15	16032652	9298054	1864884	193658	10428	260	2	17853814	11376072	2768255	308697	15431	290	1

**Tab. 4:** Table of the number of prime alternating tangles.
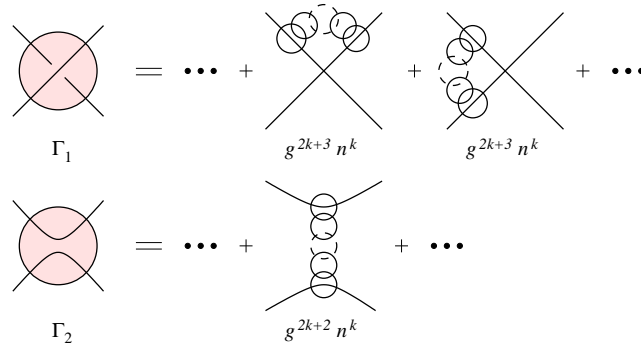
Fig. 15: Large n expansion of tangles.

The last term in each column can also be verified by means of the large n expansion. It is easy to convince oneself that in general the 2PI diagrams with the largest possible number of connected components is obtained by decorating the bare tangles by means of a festoon of chained circles, as shown on Fig. 15. In the case of Γ_1 (resp. Γ_2) there are two (resp. one) flype-inequivalent ways of doing so. As it stands, this argument holds true for odd p (resp. even p) in the case of Γ_1 (resp. Γ_2), but a similar reasoning holds true for the opposite parity. We conclude that the last term in each row of Tab. 4 should be 2 (for Γ_1

and $p \geq 6$) resp. 1 (for Γ_2 and $p \geq 2$), as is indeed observed. The next to leading terms should be obtainable in a similar fashion.

Finally, we demonstrate the power of our method by applying it to objects with more external legs. One may for example ask how many ways there are to intertwine *three* strings, and not just two as in the case of tangles. One must first establish the different ways the strings are coming out, which leads to Fig. 16.
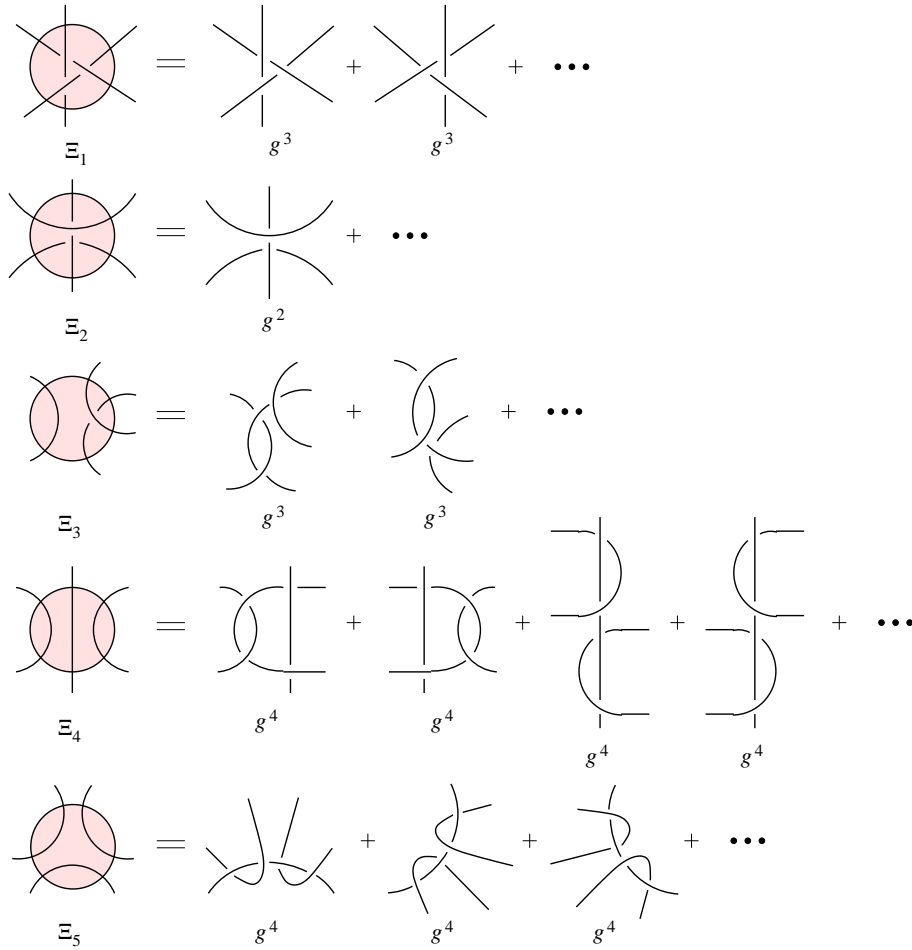
Fig. 16: The five types of tangles with 6 external legs.

We only consider configurations such that no strings can be pulled out altogether ("connected" correlation functions in the language of quantum field theory). Tab. 5 provides the first few orders of the series of the numbers of such objects.

The lowest order in p is explicited in Fig. 16. It is again relatively straightforward to check the correctness of the last entry in each row of Tab. 5 by considering the $n \to \infty$ limit. In the cases of $[\Xi_1$ with $p \geq 8]$, $[\Xi_2$ with $p \geq 7]$, and $[\Xi_3$ with $p \geq 3]$ it is straightforward

28

p \ k	Ξ_1 0	1	2	3	Ξ_2 0	1	2	3	Ξ_3 0	1	2	3	4	Ξ_4 0	1	2	3	Ξ_5 0	1	2	3
2	0				1				0					0				0			
3	2				0				2					0				0			
4	0				7				2					4				3			
5	18				6				16	2				8				9			
6	18				53	8			42	2				42	7			41	7		
7	156	24			154	6			171	44	2			156	14			168	21		
8	516	18			609	181	6		748	114	2			608	153	10		663	165	12	
9	2016	598	18		2956	422	6		2877	858	81	2		2850	586	20		3072	740	36	
10	10608	1428	18		11203	3498	318	6	14037	3752	213	2		11918	3445	364	13	13347	3966	438	18
11	40428	12318	1062	18	57664	15330	738	6	61028	19757	2511	131	2	57602	17558	1406	26	63393	20994	2040	54

Tab. 5: Table of the number of prime alternating tangles with 6 external legs.

to show that the diagrams having the highest power of g are just the trivial diagrams decorated by festoons (as in Fig. 15), meaning that the last entry in the corresponding rows should be respectively 18, 6 and 2. For the cases [Ξ_4 with $p \geq 4$] resp. [Ξ_5 with $p \geq 4$] we conjecture that the last entry of each row ξ_p should read, for p even,

$$\xi_p^{(4)} = \frac{1}{2}(3p - 4)$$
$$\xi_p^{(5)} = \frac{1}{8}(p + 8)(p - 2).$$

For p odd we have $\xi_p^{(4)} = 2\xi_{p-1}^{(4)}$ resp. $\xi_p^{(5)} = 3\xi_{p-1}^{(5)}$.

6. Discussion and outlook

In this paper we have shown how to efficiently enumerate alternating tangle diagrams with a given number of connected components and external legs, and we have explained how the flypes can be easily incorporated into our algorithm to count only topologically inequivalent objects. We have illustrated our method with numerical data that are in agreement with the exact solutions at $n = 1$ [5,6,10], $n = 2$ [7], $n = -2$ [10], and the limit $n \to \infty$, and that surpass the general results of [7] by several orders. From a computational point of view, we note that the time required to compute order p grows exponentially with p, but much more slowly than the number of diagrams counted ($\sim 2.7^p$ compared to the number of diagrams $\sim 12^p$).

A remarkable advantage of our transfer matrix algorithms is that they allow to generate planar diagrams with external legs, even in the absence of a line or closed circuit defining an obvious transfer direction.

It should be noticed that our algorithms can be straightforwardly adapted to graphs of any coordination number $q \geq 3$. For the single-step algorithm, it suffices to modify the type 1 transformation so as to insert $q - 2$ new points, instead of just two. For odd q, the parity constraints on transformation 2 no longer apply.

The geodesic algorithm can be similarly generalized. For example, on Fig. 8, changing to trivalent vertices would simply imply having five possible transformation rules instead of nine.

These generalizations open several interesting perspectives. One obvious possibility would be to numerically study matter theories defined on random graphs, by exact evaluation of correlation functions [19].
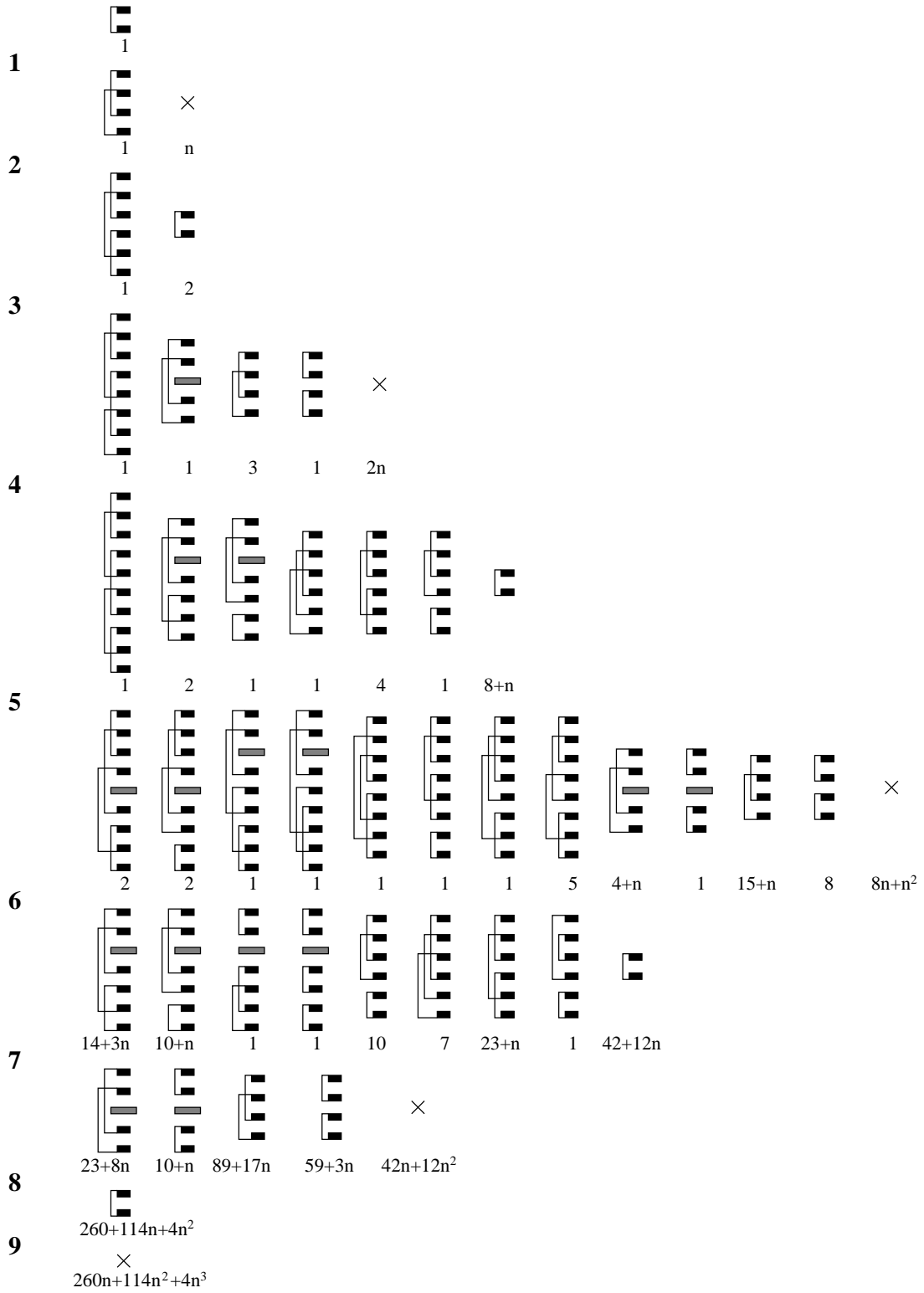
Appendix A. Tangle diagrams up to 4 crossings.

As an illustration we show on Fig. 17 the nine first iterations of the transfer matrix. We restrict ourselves to states which generate diagrams with at most four crossings. The states have all been simplified, as described in Sec. 4. The weight of the trivial state (represented by a cross on the figure) after step $2\ell - 1$ gives the number of two-legged tangle diagrams with exactly ℓ crossings, each connected component being weighed by a factor of n.[6]

---

[6] By convention, we also give a weight n to components connecting a pair of external legs, though from the point of view of diagrammatic perturbation theory this is, strictly speaking, not correct.

Fig. 17: The list of all intermediate states for tangle diagrams up to four crossings. Below each state we indicate its weight.

References

[1]   P. Di Francesco, E. Guitter and C. Kristjansen, *Integrable 2D Lorentzian Gravity and Random Walks*, *Nucl. Phys.* **B 567** (2000) 515–553 (preprint `hep-th/9907084`).

[2]   I. Jensen, *Enumerations of Plane Meanders* (preprint `cond-mat/9910313`); *A Transfer Matrix Approach to the Enumeration of Plane Meanders*, *J. Phys. A*, to appear (preprint `cond-mat/0008178`).

[3]   P. Di Francesco, E. Guitter and J.L. Jacobsen, *Exact Meander Asymptotics: a Numerical Check*, *Nucl. Phys.* **B 580** (2000) 757–795 (preprint `cond-mat/0003008`).

[4]   J. L. Jacobsen and P. Zinn-Justin, *A Transfer Matrix approach to the Enumeration of Knots* (preprint `math-ph/0102015`).

[5]   C. Sundberg and M. Thistlethwaite, *The rate of Growth of the Number of Prime Alternating Links and Tangles*, *Pac. J. Math.* **182** (1998) 329–358.

[6]   P. Zinn-Justin and J.-B. Zuber, *Matrix Integrals and the Counting of Tangles and Links*, to appear in the proceedings of the 11th International Conference on Formal Power Series and Algebraic Combinatorics, Barcelona June 1999 (preprint `math-ph/9904019`).

[7]   P. Zinn-Justin and J.-B. Zuber, *On the Counting of Colored Tangles*, *Journal of Knot Theory and its Ramifications* 9 (2000) 1127–1141 (preprint `math-ph/0002020`).

[8]   W.W. Menasco and M.B. Thistlethwaite, *The Tait Flyping Conjecture*, *Bull. Amer. Math. Soc.* **25** (1991) 403–412; *The Classification of Alternating Links*, *Ann. Math.* **138** (1993) 113–171.

[9]   P. Zinn-Justin, *Some Matrix Integrals related to Knots and Links*, proceedings of the 1999 semester of the MSRI "Random Matrices and their Applications", MSRI Publications Vol. 40 (2001) (preprint `math-ph/9910010`).

[10] P. Zinn-Justin, *The General O(n) Quartic Matrix Model and its application to Counting Tangles and Links* (preprint `math-ph/0106005`).

[11] V.A. Liskovets, *Sequence A054499* in N.J.A. Sloane (red.), *The On-Line Encyclopedia of Integer Sequences*, published electronically at http://www.research.att.com/~njas/sequences/.

[12] R. Sedgewick, *Algorithms in C* (Addison-Wesley, 1990).

[13] W.T. Tutte, *A Census of Planar Maps*, *Can. J. Math.* **15** (1963) 249–271.

[14] E. Brézin, C. Itzykson, G. Parisi and J.-B. Zuber, *Planar Diagrams*, *Commun. Math. Phys.* **59** (1978) 35–51.

[15] V.A. Kazakov and P. Zinn-Justin, *Two-Matrix Model with ABAB Interaction*, *Nucl. Phys.* **B 546** (1999) 647 (preprint `hep-th/9808043`).

[16] L. Takács, *Enumeration of rooted trees and forests*, *Math. Scientist* **18**, 1–10 (1993).

[17] V. G. Knizhnik, A. M. Polyakov and A. B. Zamolodchikov, *Fractal structure of 2D quantum gravity*, *Mod. Phys. Lett. A* **3**, 819–826 (1988); F. David, *Conformal field*

theories coupled to 2D gravity in the conformal gauge, *Mod. Phys. Lett. A* **3**, 1651–1656 (1988); J. Distler and H. Kawai, *Conformal field theory and 2D quantum gravity*, *Nucl. Phys.* **B 321**, 509 (1989).

[18] I.K. Kostov, *Mod. Phys. Lett.* A4 (1989), 217;
M. Gaudin and I.K. Kostov, *Phys. Lett.* B220 (1989), 200;
I.K. Kostov and M. Staudacher, *Nucl. Phys.* **B 384** (1992), 459.

[19] J. L. Jacobsen and P. Zinn-Justin, work in progress.